Image Denoising Based on Wavelet for IR Images Corrupted by Gaussian, Poisson & Impulse Noises

[1]Sheikh Md. Rabiul Islam, [2]Xu Huang, [3]Mingyu Liao, [4]N. K. Srinath

[1,2,3]Faculty of Education, Science, Technology &Maths, University of Canberra, Australia
[4]Department of Computer Science and Engineering, R.V. College of Engineering, India

Summery
Image denoising has remained a fundamental problem in various applications of image processing. This paper proposes a new denoising algorithm on Cohen-Daubechies-Feauveau wavelets (CDF 9/7) wavelet transform. We first applied the lifting structure to improve the drawbacks of the wavelet transform where conventional wavelet transforms and other classical decompositions seem to be restricted or limited to handle. Our proposed algorithm in this paper is very efficient in estimating and reducing noises for the contaminated images by the most popular noises such as Gaussian noise, Poisson noise and impulse (salt& pepper) noise. In this algorithm, the noisy image is first decomposed into many levels obtained from different frequency bands and then to be found the best decomposition level for the noise removal. Experimental results on several conditions are investigated for infrared images as study cases under our proposed algorithm. They are very impressive, for example under the noise with $\sigma = 0.2$ and density = 20%, for mean square error (MSE) our method decreasing 83%; peak signal to noise ratio (PSNR) increasing 98% and mean of structural similarity (MSSIM) increasing 95%, multi-scale structural similarity (MSSSIM) enhancing 93%, Feature similarity (FSIM) index growing 98.8%, Riesz-transform based Feature Similarity index (RFSIM) increasing 83.4% with the same conditions in other methods. Obviously, the experimental results shown for our proposed algorithm are significantly superior to other related methods.

Keywords:
Gaussian noise, Infrared (IR), impulse noise, MSSIM, Poisson noise.

1. Introduction

Image denoising is a procedure in digital image processing aiming at the removal of noises from the contaminated images, which may occur for an image during its acquisition or transmission. Infrared (IR) imaging has been used extensively for military and civilian purposes, in particular in dark conditions. Those applications include thermal efficiency analysis, remote temperature sensing, short-ranged wireless communication, spectroscopy, and weather forecasting. As another example, infrared astronomy uses sensor-equipped telescopes to penetrate dusty regions of space, such as molecular clouds; detect objects such as planets, and to view highly red shifted objects from the early days of the universe [1]. In our paper, it investigates the applications of infrared (IR) images encountered with various noises such as the most popular Gaussian, Poisson, and impulse (salt& pepper), noises [2]. These noises are contaminated in image acquisition, transmission, storage and processing, etc. Thus, the noises of the image could severely degrade the image quality and even cause some loss of the information from the image. Various filtering techniques have been proposed for removing image's noises by other papers. In particularly, mean & median filtering [2] have been used, the mean filter is a simple filter and it has the same construction for almost all types of noises. But this type filter has shown it may blur images and make information lost for the image. The median filter is a very effective filter in removing salt and pepper (or impulsive) noises while preserving image details. The disadvantages of this type filter are computational complexity and it will remove both the noise and fine details since this type of filters can't tell the difference between them. The adaptive median filter [3] does not perform well when the standard division of impulse noise is greater than 0.2. Gaussian filtering [4] is very effective for removing Gaussian noise. This filter is computationally efficient because large filter is implemented by small 1D filter and the degree of smoothing is controlled by the standard division σ. Also as we know that a Wiener filter [5] can only apply to an image with reasonable large standard deviation, which limited its applications in real life. Other paper works have been done on wavelet thresholding and threshold selections for image denoising become important. Donoho and Johnston [6] proposed hard- and soft-threshold methods, called VisuShrink, for denoising. However the major problem about those methods is how to make the choice of suitable threshold value. The detection of coefficients independent threshold was given by Donoho and Johnston, which depends on the noise power and the size of the images. Obviously, in real life, it is very hard to know the noise power and the size about the image before the denoising.

Wavelet transforms have received significant attentions in the field of signal and image denoising and compression. This is because of their ability to represent and analyse.

Manuscript received June 5, 2013
Manuscript revised June 20, 2013

Recently, a new wavelet construction called lifting scheme, has been developed by Wim Sweldens and Ingrid Daubechies [7]. It has also other applications, such as the possibility of defining wavelet-like transform integers to integers. In our proposed algorithm for denoising image, decomposition by lifting scheme based on Cohen-Daubechies-Feauveau (CDF) 9/7 [8] has been used to enhance the image quality with filtering methods & wavelet threshold technique. The CDF 9/7 [8] filter banks is Biorthogonal 9/7 wavelet proposed by Cohen-Daubechies-Feauveau and adopted by the JPEG2000 standard, as a core algorithm, for FBI finger print compression. The noisy in the image removed by filtering methods and wavelet threshold technique can be carried in different order. In order to obtain efficient and effective image enhancement based on evolutions by image quality matrices, the standard parameters are used such as mean average error (MAE), mean square error (MSE), the peak signal to noise ratio (PSNR) and structural similarity index (SSIM) [9], multi-scale structural similarity (MS-SSIM) [10],Feature similarity (FSIM) index [11], Riesz-transform based Feature Similarity index (RFSIM)[12] .

This paper is structured as follows. Section II describes the wavelet transform. Section III describes Cohen-Daubechies-Feauveau wavelets (CDF) 9/7 wavelet transform. In Section IV, the algorithm for denoising image is presented. Section V introduces algorithm description of denoising image. Section VI shows "Quantitative analysis". Section VIII demonstrates the simulation result & discussion. Finally, in Section IX, a conclusion is presented.

2. Wavelet Transform

The best way to describe discrete wavelet transform is through a series of cascaded filters. We first consider the FIR-based discrete transform. The input image x is fed into a two analysis filter $\tilde{h}$(low pass filter) and $\tilde{g}$(high pass filter) separately. The outputs of the two filters are then subsampled by 2. The resulting low-pass subband y_L and high-pass subband y_H are shown in Fig.1. The original signal can be reconstructed by synthesis filters h and g which take the upsampled by 2 for y_L and y_H as inputs [13]. An analysis and synthesis system has the perfect reconstruction property if and only if $x' = x$.

The mathematical representations of y_L and y_H can be defined as

$$\begin{cases} y_L(n)=\sum_{i=0}^{N_L-1}\tilde{h}(i)x(2n-i) \\ y_H(n)=\sum_{i=0}^{N_H-1}\tilde{g}(i)x(2n-i) \end{cases} \quad (1)$$

where N_L and N_H are the lengths of $\tilde{h}$ and $\tilde{g}$ respectively. For a two dimensional image, the Discrete Wavelet Transform (DWT) have to be extended to the 2D case. We suppose the image to be compressed has a dimension of M rows by N columns. The approach of the 2D implementation of the DWT is to perform the one dimensional DWT in row direction and it is followed by a one dimensional DWT in column direction. This decomposition technique is shown in Fig.2. A two dimensional row and column computation of DWT are depicted in Fig.3. In this figure, LL is a coarser version of the original image and it contains the approximation information which is in low frequency. LH, HL, and HH are the high-frequency subband containing the detail information [14]. Further computations of DWT can be performed as the level of decomposition increases. This concept is also illustrated in Fig.4. In Fig.4, the second and third level decompositions based on the principle of multiresolution analysis show that the LL1 subband in Fig.3 is decomposed into four smaller subbands: LL2, HL2, LH2, and HH2.

In order to achieve perfect reconstruction of a signal, the two channel filters shown in Fig.1 must satisfy the following conditions [7]:

$$\begin{cases} h(z)\tilde{h}(z^{-1}) + g(z)\tilde{g}(z) = 2 \\ h(z)\tilde{h}(-z^{-1}) + g(z)\tilde{g}(-z^{-1}) = 0 \end{cases} \quad (2)$$

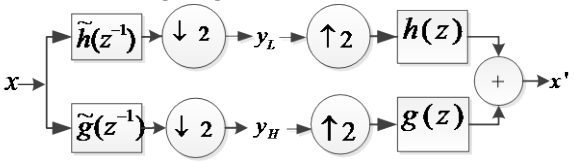

Figure 1: Discrete wavelet transform (or subband transform) analysis and synthesis system: the forward transform consists of two analysis filters h̃(low pass) and g̃(high pass) followed by subsampling 2, while the inverse transform first up samples by 2 and then uses two synthesis filters h (low pass) and g (high pass).

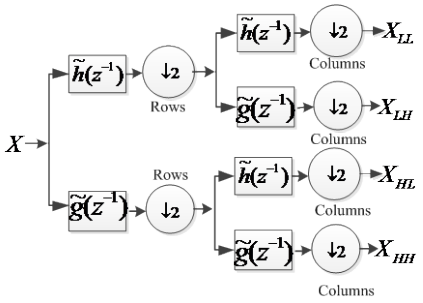

Figure 2: The 2-D DWT analysis filter bank.

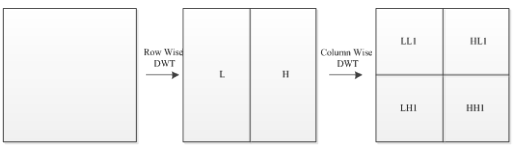

Figure 3: The two dimensional row and column computation of DWT.

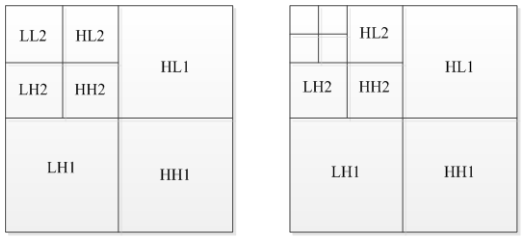

Figure 4: The (Left) second and (Right) third level row and column decomposition.

In the lifting scheme, the impulse response coefficients h and g are expressed in Laurent polynomial with the aid of Z-transform. For instance, the Laurent polynomial representation of filter h and g can be defined as

$$h(z) = \sum_{i=m}^{n} h_i z^{-i} \quad (3)$$

$$g(z) = \sum_{i=m}^{n} g_i z^{-i} \quad (4)$$

where m and n are positive integers. The analysis and synthesis filters as shown in Fig.1 are further decomposed into the polyphase representations which are expressed as

$$h(z) = h_e(z^2) + z^{-1}h_o(z^2) \quad (5)$$

$$g(z) = g_e(z^2) + z^{-1}g_o(z^2) \quad (6)$$

$$\tilde{h}(z) = \tilde{h}_e(z^2) + z^{-1}\tilde{h}_o(z^2) \quad (7)$$

$$\tilde{g}(z) = \tilde{g}_e(z^2) + z^{-1}\tilde{g}_o(z^2) \quad (8)$$

where $h_e(z) = \sum_k h_{2k} z^{-k}$ *and* $h_o(z) = \sum_k h_{2k+1} z^{-k}$ or

$$h_e(z^2) = \frac{h(z) + h(-z)}{2} \text{ and } h_o(z^2) = \frac{h(z) - h(-z)}{2z^{-1}}$$

$$g_e(z) = \sum_k g_{2k} z^{-k} \text{ and } g_o(z) = \sum_k g_{2k+1} z^{-k}$$

$$g_e(z^2) = \frac{g(z) + g(-z)}{2} \text{ and } g_o(z^2) = \frac{g(z) - g(-z)}{2z^{-1}}$$

The two polyphase matrices of the filter is defined as

$$P(z) = \begin{bmatrix} h_e(z) & g_e(z) \\ h_o(z) & g_o(z) \end{bmatrix} \quad (9)$$

$$\tilde{P}(z) = \begin{bmatrix} \tilde{h}_e(z) & \tilde{g}_e(z) \\ \tilde{h}_o(z) & \tilde{g}_o(z) \end{bmatrix} \quad (10)$$

The variable z is used since the polyphase representations are derived using Z-transform and the subscript e and o denote the even and odd sub-components of the filters which are split into sub sequences. The purpose of the polyphase representation is to reduce the computation time. The wavelet transform now is represented schematically in Fig.5. The perfect reconstruction properties is given by

$$P(z)\tilde{P}(z^{-1}) = I \quad (11)$$

where I is 2×2 identity matrix.

Now the wavelet transform can be expressed using the polyphase matrix for forward discrete wavelet transform [7], [14] is:

$$\begin{bmatrix} y_L(z) \\ y_H(z) \end{bmatrix} = \tilde{P}(z) \begin{bmatrix} x_e(z) \\ z^{-1}x_o(z) \end{bmatrix} \quad (12)$$

The inverse discrete wavelet transform becomes:

$$\begin{bmatrix} x_e(z) \\ z^{-1}x_o(z) \end{bmatrix} = P(z) \begin{bmatrix} y_L(z) \\ y_H(z) \end{bmatrix} \quad (13)$$

Finally, the upper and lower triangular matrices can be obtained by the lifting factorization process. The lifting sequences are generated by employing Euclidean algorithm which factorizes the polyphase matrix for a filter pair [7].

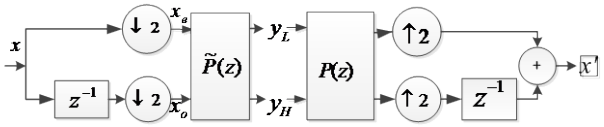

Figure 5: Ploy phase representation of wavelet transform: first subsample by 2 of input signal x into even as x_e and odd as x_o, then apply the dual polyphase matrix $\tilde{P}(z)$. For inverse transform first apply the polyphase primal matrix P(z) and then upsampled by 2 and join even and odd coefficients.

Cohen-Daubechies-Feauveau 9/7(CDF 9/7) Wavelet Transform is a lifting scheme based a wavelet transform which can reduce the computational complexity. The lifting-based WT is consists of splitting, lifting, and scaling modules and the WT itself can be treated as prediction-error decomposition. From Fig.6 we can find that it provides a complete spatial interpretation of WT. In Fig.6, let X denote the input signal and X_{L1} and X_{H1} be the decomposed output signals where they are obtained through the following three modules (*A*, *B*, and *C*) of lifting base inverse discrete wavelet transform (IDWT), which can be described as below:

A. *Splitting*-In this module, the original signal X is divided into two disjoint parts, i.e., samples $X(2n+1)$ and $X(2n)$ that denotes all odd-indexed and even-indexed samples of X , respectively [15].

B. *Lifting*-Lifting consists of three basic steps: Split, Predict, and Updating as shown below.

1. *Split* -In this stage the input signal is divided into two disjoint sets, the odd ($X[2n+1]$) and the even samples ($X[2n]$). This splitting is also called the Lazy Wavelet transform.

2. *Predict*-In this stage the even samples are used to predict the odd coefficients. This predicted value, $P(X[2n])$, is subtracted from the odd coefficients to give error in the prediction.

$$d[n] = X[2n+1] - P(X[2n]) \quad (14)$$

Here $d[n]$s are also called the detailed coefficients.

3. *Update*-In this stage, the even coefficients are combined with $d[n]$s which are passed through an update function, $U(.)$ to give

$$c[n] = X[2n] + U(d[n]) \quad (15)$$

C. *Scaling*-A normalization factor is applied to $d(n)$ and $c(n)$, respectively. In the even-indexed part $c(n)$ is multiplied by a normalization factor K_e to produce the wavelet sub band X_{L1}. Similarly in the odd-index

part the error signal $d(n)$ is multiplied by K_o to obtain the wavelet sub band X_{H1}.

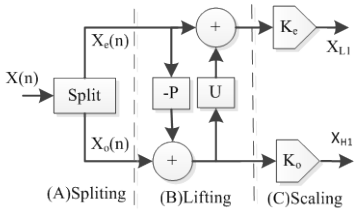

Figure 6: The lifting-based WT [15].

The Lifting scheme based Cohen-Daubechies-Feauveau (CDF) 9/7 wavelet transform goes through of four steps: two prediction operators ('a' and 'b') and two update operators ('c' and 'd') as shown in Fig.7. The analysis filter $\tilde{h}$ has nine coefficients, while the synthesis filter has seven coefficients. Both high pass filters g , $\tilde{g}$ have four vanishing moments. We chose the filter with seven coefficients filter because it gives the rises to a smoother scaling function than the nine coefficients. In this fact, we run the factoring algorithm starting from the analysis filter [7]:

$\tilde{h}_e(z) = h_4(z^2 + z^{-2}) + h_2(z + z^{-1}) + h_o$ and $\tilde{h}_o(z) = h_3(z^2 + z^{-2}) + h_1(z + 1)$

$\tilde{g}_e(z) = -g_o - g_2(z + z^{-1})$ and $\tilde{g}_o(z) = g_1(1 + z^{-1}) + g_3(z + z^{-1})$

The coefficients of the remainders are computed as:

$$r_o = h_o - 2h_4h_1/h_3$$
$$r_1 = h_2 - h_4 - h_4h_1/h_3$$
$$s_o = h_1 - h_3 - h_3r_o/r_1$$

If we now let

$$a = h_4/h_3 \approx -1.58613432,$$
$$b = h_3/r_1 \approx -0.05298011854,$$
$$c = r_1/s_o \approx 0.8829110762,$$
$$d = s_o/r_o \approx 0.4435068522,$$
$$K = r_o - 2r_1 \approx 1.149604398.$$

Since the 9/7 tape wavelet filter is symmetric we can present h and g in the z-domain. Hence, a poly-phase matrix $\tilde{P}(z)$ presents the filter pair(h, g):

$$\tilde{P}(z) = \begin{bmatrix} \tilde{h}_e(z) & \tilde{g}_e(z) \\ \tilde{h}_o(z) & \tilde{g}_o(z) \end{bmatrix}$$
$$= \begin{bmatrix} h_4(z^2 + z^{-2}) + h_2(z + z^{-1}) + h_o & g_1(1 + z^{-1}) + g_3(z + z^{-1}) \\ h_3(z^2 + z^{-2}) + h_1(z + 1) & g_1(1 + z^{-1}) + g_3(z + z^{-1}) \end{bmatrix}$$

Then, we use factorization algorithm is given by

$$\tilde{P}(Z) = \begin{bmatrix} 1 & a(1 + Z^{-1}) \\ 0 & 1 \end{bmatrix} \cdot \begin{bmatrix} 1 & 0) \\ b(1 + Z) & 1 \end{bmatrix} \cdot \begin{bmatrix} 1 & c(1 + Z^{-1}) \\ 0 & 1 \end{bmatrix} \cdot \begin{bmatrix} 1 & 0) \\ d(1 + Z) & 1 \end{bmatrix} \cdot \begin{bmatrix} K & 0 \\ 0 & 1/K \end{bmatrix} \quad (16)$$

We have found that the four "lifting" steps and the two "scaling" steps from Fig.7 are with same parameter as follows:

$$\begin{cases} Y(2n+1) \leftarrow X(2n+1) + (\mathrm{a} \times [\mathrm{X}(2\mathrm{n}) + \mathrm{X}(2\mathrm{n}+2)]) \\ Y(2n) \leftarrow X(2n) + (\mathrm{b} \times [\mathrm{Y}(2\mathrm{n}-1) + \mathrm{Y}(2\mathrm{n}+1)]) \\ Y(2n+1) \leftarrow Y(2n+1) + (\mathrm{c} \times [\mathrm{Y}(2\mathrm{n}) + \mathrm{Y}(2\mathrm{n}+2)]) \\ Y(2n) \leftarrow Y(2n) + (\mathrm{d} \times [\mathrm{Y}(2\mathrm{n}-1) + \mathrm{Y}(2\mathrm{n}+1)]) \end{cases} \quad (17)$$

$$\begin{cases} Y(2n+1) \leftarrow K \times Y(2n+1), \\ Y(2n) \leftarrow \left(\frac{1}{\mathrm{K}}\right) \times Y(2n), \end{cases} \quad (18)$$

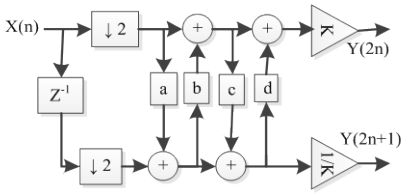

Figure 7: Lifting scheme of the analysis side of the CDF 9/7 filter bank.

The synthesis side of the CDF9/7 filter bank simply inverts the scaling, and reverses the sequence of the lifting and update steps. Fig.8 shows the synthesis side of the filter bank using lifting structure to reconstruct of the signal or image.

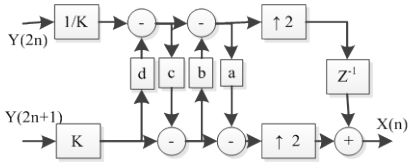

Figure 8: Lifting implementation of the synthesis side of the CDF 9/7 filter bank.

3. Denoising Image

The objective of CDF 9/7 wavelet based denoising process is to estimate the original image $x(i,j)$ by discarding the corrupted noise $e(i,j)$ from the function$f(i,j)$:

$$f(i,j) = x(i,j) + e(i,j) \quad (19)$$

The threshold value is computed for denoising images into the noisy images $f(i,j)$ by the medium absolute deviation (MAD) was proposed by Donoho and Johnston [6]. It's called the universal 'VisuShrink' threshold given by [6]:

$$Thr = \sigma\sqrt{2.log(N)} \quad (20)$$

The noise variance is estimated using the mean absolute deviation (MAD) method and is given by

$$\sigma^2 = \left(\frac{MAD(|c_{i,j}|)}{0.6754}\right)^2 \quad (21)$$

where $c_{i,j}$ is the wavelet coefficient of the noisy image. Two wavelet thresholding techniques like *hard thresholding and soft thresholding* have provided better efficiency in image denoising based on universal threshold. The hard thresholding T_H can be defined as [6]

$$T_H = \begin{cases} x & for\ |x| \geq Thr \\ 0 & in\ all\ other\ regions \end{cases} \quad (22)$$

The soft thresholding T_s can be defined as follows [6],

$$T_s = \begin{cases} sign(x)(|x| - Thr) & for\ |x| > Thr \\ 0\ in\ all\ other\ regions \end{cases} \quad (23)$$

The wavelet based denoising process follows resulting DWT detail coefficients are threshold by shrinkage (soft, hard). The original IR images can be reconstructed from the threshold wavelet, whose detail coefficients show a denoised (smoothed) version of the original images.

4. Denoising Algorithm Description

The denoising algorithm is designed to the noisy infrared (IR) images corrupted by multi-noise, particularly by the most popular noises: Gaussian Noise, Poisson noise, and impulse (slat & pepper) noise. The flow chart of our proposed algorithm is shown in Fig. 9.

Our proposed denoising algorithm can be summarized as below:

Step.1 Reading the infrared (IR) images on the workspace of the MATLAB.

Step.2 Adding Gaussian noise, Poisson noise, and impulse (slat & pepper) noise in IR images with noise variance with three cases: case 1. Noise variance =0.1 & noise density=10%, case 2. Noise variance=0.2, Noise density=20%, and case 3. Noise variance=0.025, Noise density=2.5%.

Step.3 Performing CDF9/7 wavelet transforms to the IR images: from the decomposition process the coefficients can be extracted. We have tested with different decomposing level 1, 2, 3, 4…20(as we considered) and found the level 3 comments on the quality of images with original images.

Step.4 Estimating the noise variance for each noisy image pixel [refer to equation (21)].

Step.5 The threshold T for the wavelet coefficients of noisy image is calculated by equation (22 & 23).

Step.6 If the wavelet coefficients are greater than threshold (Thr), then coefficients are remained unchanged. Otherwise, they are suppressed.

Step.7 Then, further comparing for denoising image: applying kernel mask, size 3x3 of median filtering, Gaussian filtering and Wiener filters individually.

Step.8 After above, all the resultant coefficients are reconstructed by applying inverses CDF 9/7 wavelet transform, which results in deionised image.

Step.9 Calculate MAE, MSE, PSNR, MSSIM, MSSSIM, FSIM, and RFSIM to find out the best quality denoised image.

Step.10 The same process is repeated for various IR images and compares its performance.

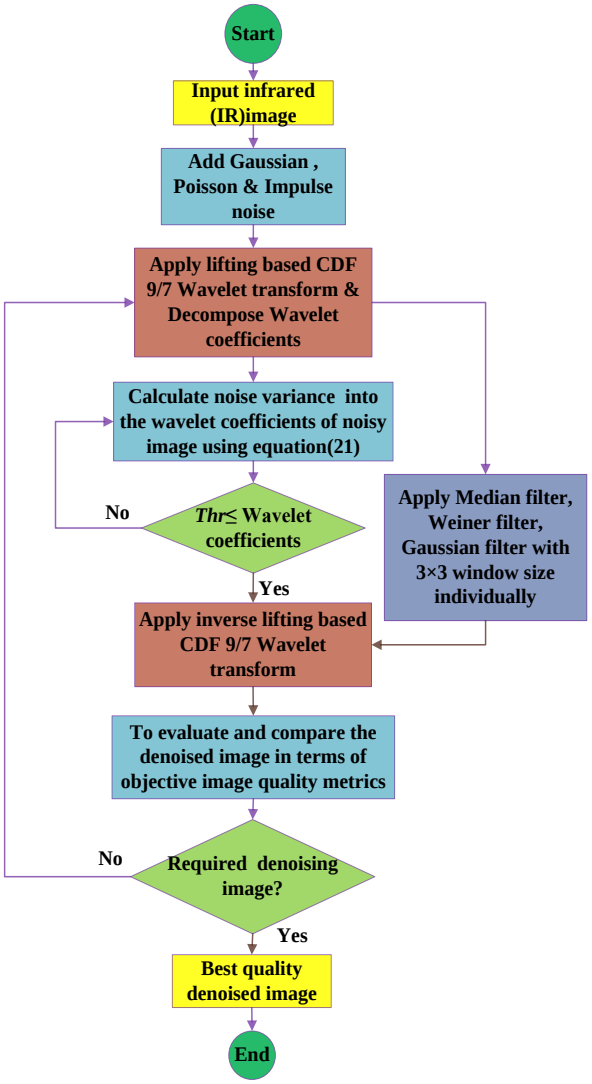

Figure 9: Flow chart of proposed denosing algorithm.

5. Quantitative Analysis

Let x_i and y_i be the i^{th} pixel in the original image x and degraded image y, respectively. The MSE and PSNR between two images are given by

$$MSE = \frac{1}{N}\sum_{i=1}^{N}(x_i - y_i))^2 \quad (24)$$

$$PSNR = 10log_{10}\frac{(2^n-1)^2}{\sqrt{MSE}} \quad (25)$$

Where N is the total number of pixels in the image and n=8 bit/pixel gray scale images.

Apart from the PSNR assessment, the mean of absolute error (MAE) has also been used in an analysis to characterize the filter's detail preservation behaviour, one which is defined by:

$$MAE = \frac{1}{M\times N}\sum_{i=1}^{i=M}\sum_{j=1}^{j=N}(x(i,j) - y(i,j)) \quad (26)$$

Following [9] , we also defined the *structural similarity index (*SSIM*)* for estimating the quality of IR images.We assessed a new model to estimate the quality of infrared images, specifically for the ones decomposed and reconstruction by CDF 9/7 wavelet transform. This is based on the hypothesis that the human visual system (HVS) is highly adapted to extract structural information. In fact, the spatial domain SSIM compares the reference image with degraded image on the image's brightness, contrast and structure. The SSIM index define as the product of three components which gives

$$SSIM(x,y) = \frac{(2\mu_x\mu_y+C_1)(2\sigma_x\sigma_y+C_2)}{(\mu_x^2+\mu_y^2+C_1)(\sigma_x^2+\sigma_y^2+C_2)} \quad (27)$$

In real application, it is required the average of overall measurement of the whole image quality, which is defined as mean structural similarity index (MSSIM) and given by below:

$$MSSIM\ (X,Y) = \frac{1}{M}\sum_{i=1}^{M} SSIM(x_i, y_i) \quad (28)$$

where *X* and *Y* are respectively the reference and degraded images, $x_i\ and\ y_i$ are the contents of images at the i^{th} local window. *M* is the total number of local windows in image.

The multi-scale extension of SSIM, called MS-SSIM [10] , produced better results than its single-scale counterpart. Conceptually, this work related to the contrast sensitivity function (CSF) of the Human Vision System (HVS). The HVS measured weight function peaks at middle-resolution scales and drops at both low and high resolution scales .The overall MS-SSIM measure is defined as

$$MS-SSIM = \prod_{j=1}^{M}\left(SSIM_j\right)^{\beta_j} \quad (29)$$

where the β_j values were obtained through psychophysical measure at the scale M.

The Feature Similarity (FSIM) [Reader read the reference [11]] index have calculated the similarity between images f_1 and f_2. Denoted by PC_1 and PC_2 the phase congruency (PC) maps extracted features from f_1 and f_2 ,as well as G_1 and G_2 the gradient magnitude (GM) maps extracted features from them. The PC is contrast invariant but image local contrast does not affect HVS perception on the image quality. The image gradient magnitude (GM) is computed as the secondary feature to encode contrast information. The FSIM index in defines as

$$FSIM = \frac{\sum_{x\in\Omega} S_L(x).PC_m(x)}{\sum_{x\in\Omega} PC_m(x)} \quad (30)$$

Where $PC_m(x) = \max\left(PC_1(x), PC_2(x)\right)$ to weight the importance of $S_L(x)$ in the overall similarly between f_1 and f_2.

Another novel IQA metric, namely Riesz-transform based Feature Similarity (RFSIM) index [12]. RFSIM is computed by comparing Riesz transform features at key locations between the reference images and distorted images. Considered HVS is sensitive to image edges; key locations are masked by a mask formed by the Canny operator. For feature extraction, 1st and 2nd order Riesz transform are used .They can easily extract several types of image low-level features effectively and efficiently in theoretical framework.

The similarity between two feature maps f_i ($i = 1\sim5$) and g_i at the corresponding location (*x*, *y*) is defined as

$$d_i(x,y) = \frac{2f_i(x,y).g_i(x,y)+c}{f_i^2(x,y)+g_i^2(x,y)+c} \quad (31)$$

where c is a small constant value.

The RFSIM index between f and g by considering only the key locations marked by mask *M is* defined as

$$RFSIM = \prod_{i=1}^{5} \frac{\sum\sum d_i(x,y).M(x,y)}{\sum\sum M(x,y)} \quad (32)$$

6. Results & Discussion

In this section we present some simulation results performed on the infrared images and implemented in MATLAB under our proposed denoising algorithm. In order to make good comparisons, our proposed algorithm was with different filter methods and wavelet thresholding techniques for denoising infrared image. We have taken an infrared (IR) images in standard parameters, such as size 500×500 encoded on 8 bits per pixel, which was taken from the open database [16]. Tables 1-7 and also Figs 10-15 showed the values of image quality comparison on the values of objective quality matrices such as MAE, MSE, PSNR, MSSIM, MS-SSIM, FSIM, and RFSIM. The experimental results have been shown in Figs 13(b), 14 (b) and 15 (b), which demonstrated the best performance in proposed denoising image algorithm for the infrared images corrupted with Gaussian noise, Poisson noise, and impulse noises (salt& pepper).We have used different filters for denoising infrared image. All the tables represented the values of MAE, MSE, PSNR, MSSIM, MS-SSIM, FSIM, and RFSIM at the different noise variances, such as $\sigma = 0.025,\ 0.1, 0.2$ for the Gaussian noise, Poisson noise with $\lambda = 0.9686$ and impulse (salt & pepper) noise with different densities, *ND*, and *ND* = 2.5%, 10% and 20%. The various filters are used to compare the performances of median filter, Gaussian filter, Wiener filter, soft and hard threshold technique. The best result was in bold font. It has shown the highest PSNR value with minimum MSE & MAE value, which, as expected, depended on the lower value of noise variances for Gaussian noise, means of Poisson noise and noise densities for impulse noise of the entire image. A visual inspection was carried out in order to judge the filters' effectiveness in reducing Gaussian noise, Poisson noise & impulse noise effect as shown in Figs.16(c), 17(c) & 18(c). We can conclude that the value of an output pixel is determined by the median of the neighbourhood pixels, rather than the mean. We also observed that the median filter is much less sensitive than the mean filter to the extreme values (called *outliers*). Median filtering is therefore better way being able to remove these outliers without reducing the sharpness of the image. Results obtained by the median

filter, with size 3x3, are shown in Figs. 16(c), 17(c) & 18(c). The Wiener filtering gave the optimal results in terms of the mean square error. The results of the noised removed for the contaminated IR image by Wiener filter or adaptive median filter, with size 3×3, are shown in Figs 16(d), 17(d) & 18(d). These filters are applied by low-pass filters convolution kernel with a small window size 3×3 and a standard deviation $\sigma = 4$. The results of noise elimination based on their gray-level value as shown in Figs. 16(e), 17(e) & 18(e). The MAE, MSE, PSNR, MSSIM, MS-SSIM, FSIM, and RFSIM results for the image denoising by the wavelet thresholding techniques have been shown in tables, which are considerably worse than the other filtering methods, as shown in Figs.16 (g) & (f), 17 (g) & (f), & 18 (g) & (f). It is clear from results listed on tables 1-7 that the median filter method removed the noise significantly for the quality metrics such as MAE, MSE, PSNR, MSSIM, MS-SSIM, FSIM, and RFSIM. The median filter tends to smooth the image, thereby could be losing some details (e.g. sharp edges) of the original signal which can result in an increased estimation error.

Table.1 Comparison of MAE values for different filters at infrared (IR) image corrupted by Gaussian, Poisson & impulse (salt& pepper) noise

Filter algorithm	$\sigma = 0.025$ $\lambda = 0.9686$ $ND = 2.5\%$	$\sigma = 0.1$ $\lambda = 0.9686$ $ND = 10\%$	$\sigma = 0.2$ $\lambda = 0.9686$ $ND = 20\%$
	MAE	MAE	MAE
Noisy image	0.5636	0.5804	0.6020
Proposed algorithm	**0.5580**	**0.5600**	**0.5705**
Wiener filter	**0.5633**	0.5794	0.6021
Gaussian filter	0.5627	0.5788	0.6015
Hard threshold	0.3959	0.4204	0.4527
Soft threshold	6.0844e-04	0.0143	0.0350

Table.2 Comparison of MSE values for different filters at infrared (IR) image corrupted by Gaussian, Poisson & impulse (salt& pepper) noise

Filter algorithm	$\sigma = 0.025$ $\lambda = 0.9686$ $ND = 2.5\%$	$\sigma = 0.1$ $\lambda = 0.9686$ $ND = 10\%$	$\sigma = 0.2$ $\lambda = 0.9686$ $ND = 20\%$
	MSE	***MSE***	***MSE***
Noisy image	0.5386	0.5768	0.6450
Proposed algorithm	**0.5243**	**0.5256**	**0.5363**
Wiener filter	0.5282	0.5392	0.5569
Gaussian filter	0.5220	0.5292	0.5444
Hard threshold	0.5068	0.5451	0.6092
Soft threshold	0.0541	0.0649	0.0866

Table.3 Comparison of PSNR values for different filters at infrared (IR) image corrupted by Gaussian, Poisson & impulse (salt& pepper) noise

Filter algorithm	$\sigma = 0.025$ $\lambda = 0.9686$ $ND = 2.5\%$	$\sigma = 0.1$ $\lambda = 0.9686$ $ND = 10\%$	$\sigma = 0.2$ $\lambda = 0.9686$ $ND = 20\%$
	PSNR (dB)	***PSNR (dB)***	***PSNR (dB)***
Noisy image	50.8169	50.5268	50.0398
Proposed algorithm	**50.9323**	**50.9205**	**50.8472**
Wiener filter	50.8994	50.8150	50.6803
Gaussian filter	50.9501	50.8965	50.7779
Hard threshold	51.0769	50.7651	50.2749
Soft threshold	60.7922	60.0226	58.7919

Table.4 Comparison of MSSIM values for different filters at infrared (IR) image corrupted by Gaussian, Poisson & impulse (salt& pepper) noise

Filter algorithm	$\sigma = 0.025$ $\lambda = 0.9686$ $ND = 2.5\%$	$\sigma = 0.1$ $\lambda = 0.9686$ $ND = 10\%$	$\sigma = 0.2$ $\lambda = 0.9686$ $ND = 20\%$
	MSSIM	***MSSIM***	***MSSIM***
Noisy image	0.9432	0.9417	0.9393
Proposed algorithm	**0.9704**	**0.9943**	**0.9898**
Wiener filter	0.9435	0.9423	0.9408
Gaussian filter	0.9435	0.9149	0.9410
Hard threshold	0.9438	0.9301	0.9783
Soft threshold	0.9436	0.9435	0.9429

Table.5 Comparison of MS-SSIM values for different filters at infrared (IR) image corrupted by Gaussian, Poisson & impulse (salt& pepper) noise

Filter algorithm	$\sigma = 0.025$ $\lambda = 0.9686$ $ND = 2.5\%$	$\sigma = 0.1$ $\lambda = 0.9686$ $ND = 10\%$	$\sigma = 0.2$ $\lambda = 0.9686$ $ND = 20\%$
	MS-SSIM	***MS-SSIM***	***MS-SSIM***
Noisy image	0.9158	0.9150	0.9138
Proposed algorithm	**0.9551**	**0.9940**	**0.9874**
Wiener filter	0.9158	0.9151	0.9140
Gaussian filter	0.9158	0.9151	0.9140
Hard threshold	0.9167	0.9302	0.9778
Soft threshold	0.9159	0.9158	0.9154

Table.6 Comparison of FSIM values for different filters at infrared (IR) image corrupted by Gaussian, Poisson & impulse (salt& pepper) noise

Filter algorithm	$\sigma = 0.025$ $\lambda = 0.9686$ $ND = 2.5\%$	$\sigma = 0.1$ $\lambda = 0.9686$ $ND = 10\%$	$\sigma = 0.2$ $\lambda = 0.9686$ $ND = 20\%$
	FSIM	***FSIM***	***FSIM***
Noisy image	0.9986	0.9927	0.9803
Proposed algorithm	**0.9990**	**0.9979**	**0.9923**
Wiener filter	0.9988	0.9952	0.9872
Gaussian filter	0.9985	0.9958	0.9887
Hard threshold	0.9965	0.9783	0.9470
Soft threshold	0.9957	0.9745	0.9497

Table.7 Comparison of FSIM values for different filters at infrared (IR) image corrupted by Gaussian, Poisson & impulse (salt& pepper) noise

Filter algorithm	$\sigma = 0.025$ $\lambda = 0.9686$ $ND = 2.5\%$	$\sigma = 0.1$ $\lambda = 0.9686$ $ND = 10\%$	$\sigma = 0.2$ $\lambda = 0.9686$ $ND = 20\%$
	RSIM	***RSIM***	***RSIM***
Noisy image	0.7752	0.7820	0.7874
Proposed algorithm	**0.8127**	**0.9164**	**0.9557**
Wiener filter	0.7793	0.7894	0.8027
Gaussian filter	0.7807	0.7911	0.8051
Hard threshold	0.7559	0.6848	0.7081
Soft threshold	0.7744	0.7758	0.7808

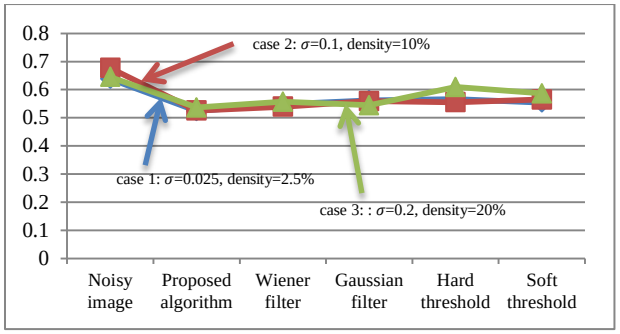

Figure 10: Comparisons of MSE values for different filters at IR image corrupted by Gaussian, Poisson and impulse noise. It is obviously the proposed algorithm has the minimum MSE in all the three different cases.

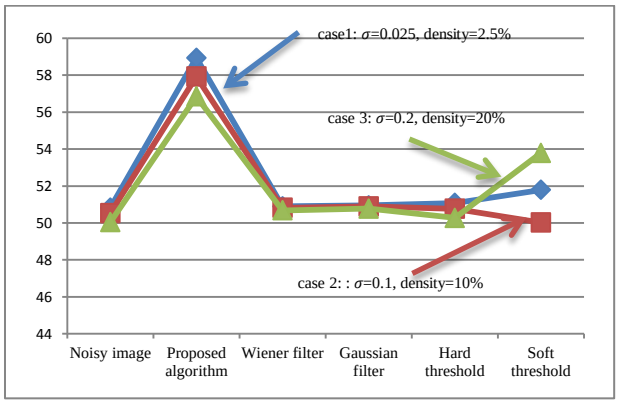

Figure 11: Comparisons of PSNR values for different filters at IR image corrupted by Gaussian, Poisson and impulse noise. It is clearly the proposed algorithm has the maximum PSNR in all the three different cases.

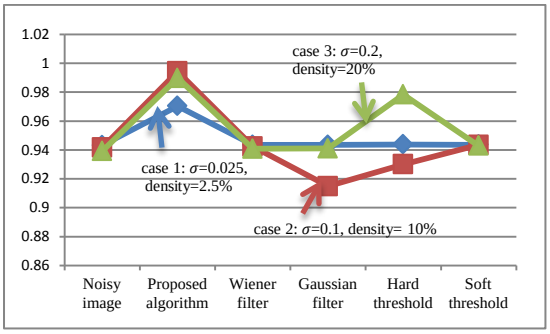

Figure 12: Comparisons of MSSIM values for different filters at IR image corrupted by Gaussian, Poisson and impulse noise. It is clearly the proposed algorithm has the maximum MSSIM in all the three different cases.

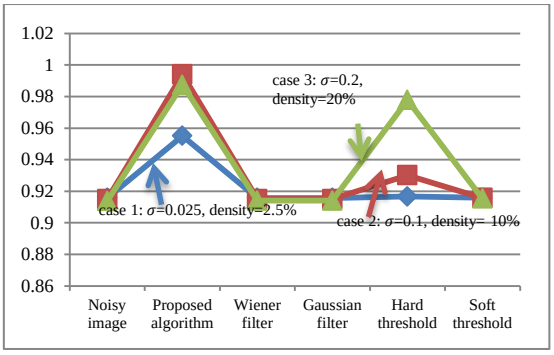

Figure 13: Comparisons of MSSSIM values for different filters at IR image corrupted by Gaussian, Poisson and impulse noise. It is clearly the proposed algorithm has the maximum MSSSIM in all the three different cases.

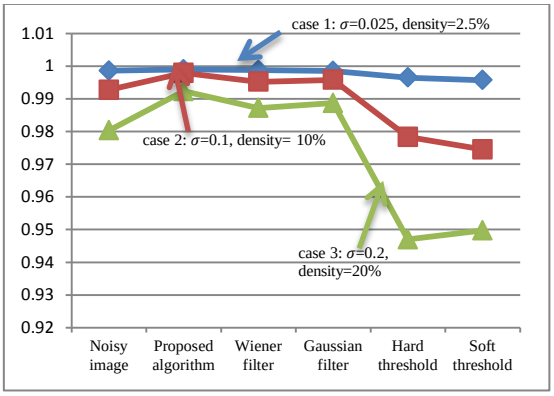

Figure 14: Comparisons of FSIM values for different filters at IR image corrupted by Gaussian, Poisson and impulse noise. It is clearly the proposed algorithm has the maximum FSIM in all the three different cases.

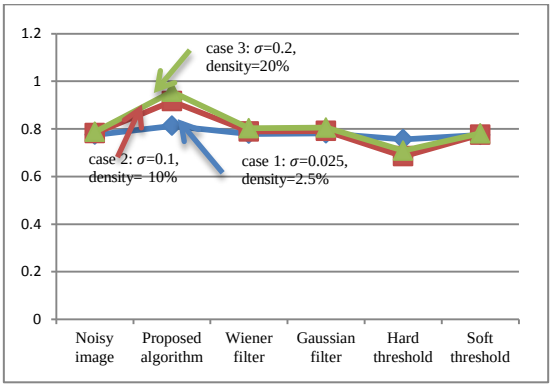

Figure 15: Comparisons of RSIM values for different filters at IR image corrupted by Gaussian, Poisson and impulse noise. It is clearly the proposed algorithm has the maximum RSIM in all the three different cases.

We use three evaluation metrics to compare the performance of proposed denoising image and original image. The first two metrics are the Spearman rank order

correlation coefficient (SROCC) and the Kendall rank order correlation coefficient (KROCC) is employed to assess monotonicity. The third metric is the Pearson linear correlation coefficients (PLCC) between the mean opinion score (MOS) and the objective score after nonlinear regression [17]. In our work we have used open souses infrared images database. They don't identify the MOS scores and objective scores. We have only used this three metrics from MATLAB optimization toolbox for compare the performance of image denoising. Since all the reference images are assumed to have perfect quality. There are no natural relative ranks between them in resulting ambiguities when computing the SROCC, KROCC, and PLCC. Tables 8-10 gives the results of SROCC, KROCC, and PLCC over the original infrared image and denoised image that was corrupted by three different noises such as Gaussian noise, Poisson noise and impulse noise. We can clearly see through the results in tables 8-10 that the proposed denoising image by median filter as bold font much better than all other filtering methods. It has evaluated in terms of all the three evaluation metrics.

Table.8 Comparison of Spearman rank correlation coefficient (SROCC) values for different filters at infrared (IR) image corrupted by Gaussian, Poisson & impulse (salt& pepper) noise

Filter algorithm	$\sigma = 0.025$ $\lambda = 0.9686$ $ND = 2.5\%$	$\sigma = 0.1$ $\lambda = 0.9686$ $ND = 10\%$	$\sigma = 0.2$ $\lambda = 0.9686$ $ND = 20\%$
	SROCC	***SROCC***	***SROCC***
Noisy image	0.9489	0.8562	0.7617
Proposed algorithm	**0.9635**	**0.9407**	**0.9237**
Wiener filter	0.9574	0.9127	0.8868
Gaussian filter	0.9559	0.9281	0.9078
Hard threshold	0.9196	0.7151	0.3126
Soft threshold	0.9196	0.7151	0.3126

Table.9 Comparison of Kendall rank correlation coefficient (KROCC) values for different filters at infrared (IR) image corrupted by Gaussian, Poisson & impulse (salt& pepper) noise

Filter algorithm	$\sigma = 0.025$ $\lambda = 0.9686$ $ND = 2.5\%$	$\sigma = 0.1$ $\lambda = 0.9686$ $ND = 10\%$	$\sigma = 0.2$ $\lambda = 0.9686$ $ND = 20\%$
	KROCC	***KROCC***	***KROCC***
Noisy image	0.8422	0.7098	0.5980
Proposed algorithm	**0.8759**	**0.8303**	**0.7909**
Wiener filter	0.8661	0.7908	0.7356
Gaussian filter	0.8603	0.8081	0.7617
Hard threshold	0.8257	0.5913	0.2610
Soft threshold	0.8257	0.5913	0.2610

Table.10 Comparison of Pearson linear correlation coefficients(PLCC) values for different filters at infrared (IR) image corrupted by Gaussian, Poisson & impulse (salt& pepper) noise

Filter algorithm	$\sigma = 0.025$ $\lambda = 0.9686$ $ND = 2.5\%$	$\sigma = 0.1$ $\lambda = 0.9686$ $ND = 10\%$	$\sigma = 0.2$ $\lambda = 0.9686$ $ND = 20\%$
	PLCC	***PLCC***	***PLCC***
Noisy image	0.9809	0.9060	0.7918
Proposed algorithm	**0.9900**	**0.9877**	**0.9712**
Wiener filter	0.9838	0.9650	0.9325
Gaussian filter	0.9897	0.9816	0.9611
Hard threshold	0.9727	0.8101	0.3965
Soft threshold	0.9566	0.7474	0.3080

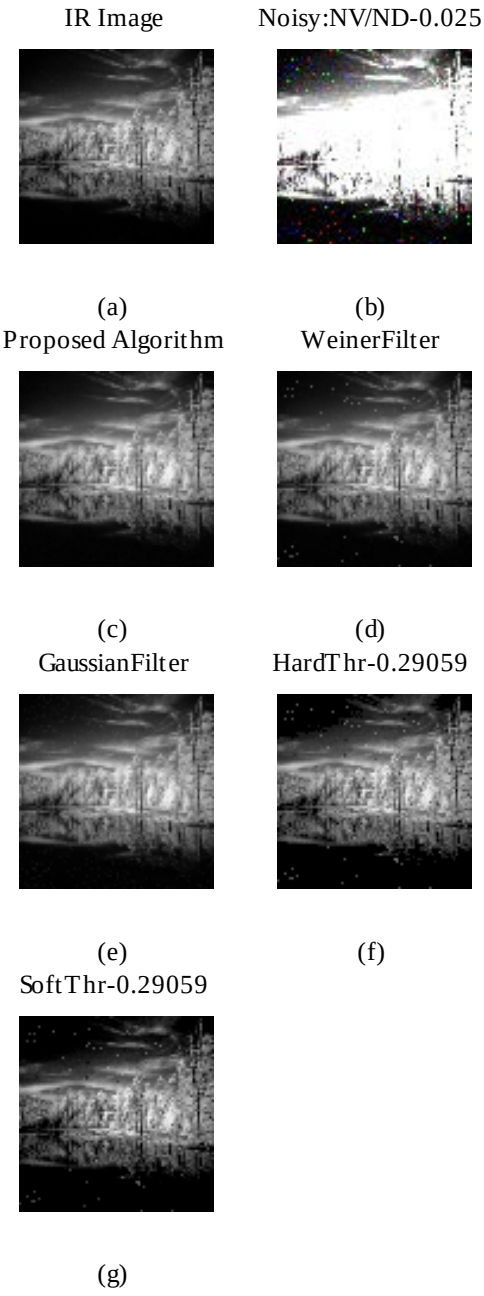

Figure 16: Denoising of IR image (a) Original image (b) Noisy image (noise variance=0.025 for Gaussian and $\lambda = 0.9686$ for Poisson noise and 2.5% noise density for impulse noise) (c) Denoised image with Median filter (d) Denoised image with Wiener filter (e) Denoised image with Gaussian filter (f) Denoised image with hard threshold (g) Denoised image with soft threshold.

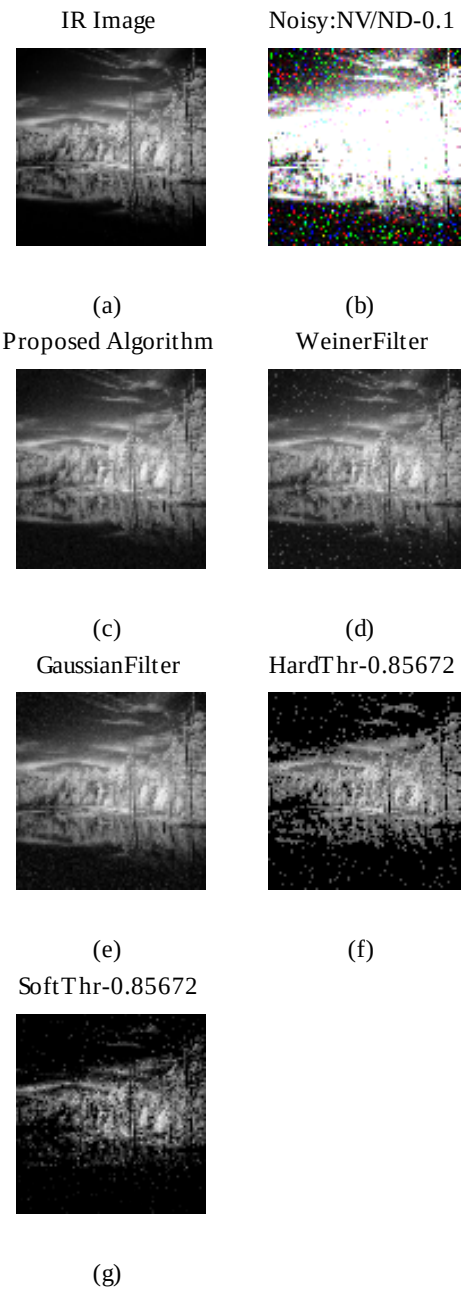

Figure 17: Denoising of IR image (a) Original image (b)Noisy image(noise variance=0.1for Gaussian and $\lambda = 0.9686$ for Poisson noise and 10% noise density for impulse noise) (c) Denoised image with Median filter (d) Denoised image with Wiener filter (e) Denoised image with Gaussian filter($\sigma = 4$) (f) Denoised image with hard threshold (g) Denoised image with soft threshold.

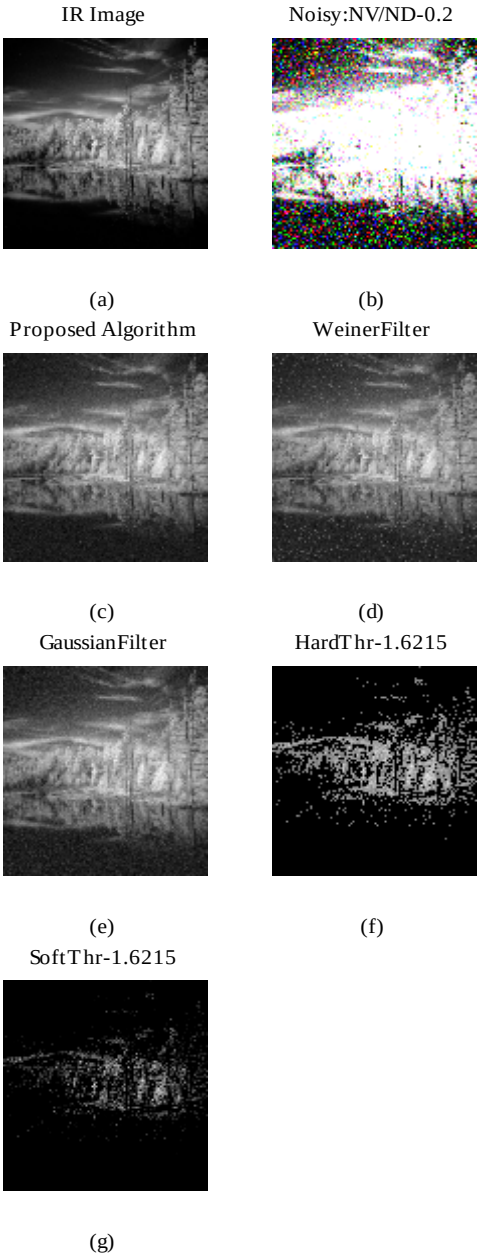

Figure 18: Denoising of IR image (a) Original image (b)Noisy image(noise variance=0.2 for Gaussian and $\lambda = 0.9686$ for Poisson noise and 20% noise density for impulse noise) (c) Denoised image with Median filter (d) Denoised image with Wiener filter (e) Denoised image with Gaussian filter($\sigma = 4$) (f) Denoised image with hard threshold (g) Denoised image with soft threshold.

7. Conclusion

In this paper, a simple effective and efficient denoising algorithm is proposed based on wavelet technology. Our previous research [18] has been extended to the image recovery from an IR image corrupted with multi-noise, in particularly for the three major popular IR image's noises, Gaussian noise, Poisson noise & impulse noise. The evaluation of the results supports the fact that our proposed algorithm has significantly improved noise removal result than others methods. For example, under the noise with $\sigma = 0.2$ and density = 20% cases for our proposed algorithm, the MSE is decreasing 83%; peak signal to noise ratio (PSNR) increasing 98% and mean of structural similarity (MSSIM) increasing 95%, multi-scale structural similarity (MS-SSIM) enhancing 93%, Feature similarity (FSIM) index growing 98.8%, Riesz-transform based Feature Similarity index (RFSIM) increasing 83.4% under the same conditions. The proposed algorithm presented better results with smoothness and better edge preservation at the same subband coefficients. Our research also demonstrated that the noise removal significantly depends on the minimum value of the noise density for different filters such as median filter, Gaussian filter, Wiener filter and soft and hard thresholding. Moreover, it further suggested that a threshold may be implemented to the compression framework, which may further improve the denoising performance.

Acknowledgement

This project is supported by the Australian Academy of Science, Australia-India Fellowships 2012-2013.

References

[1] A. Sahu and V. Shandilya, "Infrared Image Enhancement Using Wavelet Transform," Computer Engineering and Intelligent Systems, vol. 3, no. 3, pp. 40–47, Feb. 2012.

[2] Abreu, M. Lightstone, S.K. Mitra and K. Arakawa, "A New Efficient Approach for the Removal of Impulse Noise from Highly Corrupted Images," IEEE Trans. Image Processing, vol. 5, no. 6, pp. 1012–1025, Jun. 1996.

[3] Sawant, H.Zeman, D. Muratone, S. Samant and F. DiBianca, "Adaptive median filter algorithm to remove impulse noise in x-ray and CT images and speckle in ultrasound images," Medical Imaging 99., Proc SPIE 3661, pp. 1263–1274, 1999.

[4] KOVESI, P.D., "Fast Almost-Gaussian Filtering"," presented at the 2010 International Conference on Digital Image Computing: Techniques and Applications (DICTA), Sydney, Australia, 2010, vol. E4271, pp. 121 – 125.

[5] I. Ahmad, P. P. Mondal, and R. Kanhirodan, "A New FIR Filter for Image Restoration," in 1ST IEEE Conference on Industrial Electronics and Applications, 2006, pp. 1–6.

[6] D. L. Donoho, "De-noising by soft-thresholding," IEEE Transactions on Information Theory, vol. 41, no. 3, pp. 613 –627, May 1995.

[7] Ingrid Daubechies, W. Sweldens, "Factoring Wavelet Transforms into Lifting Steps," Journal of Fourier analysis and Applications, vol. 4, no. 3, pp. 247 – 269, May 1998.

[8] A. Cohen, I. Daubechies, and J.C. Feauveau, "Biorthogonal bases of compactly supported wavelets," Comm. Pure & Appl. Math., vol. 45, no. 5, pp. 485–560, 1992.

[9] Zhou Wang, Alan C. Bovik,Hamid R. Sheikh, Eero P. Simoncelli, "Image Quality Assessment: From Error Visibility to Structural Similarity," IEEE TRANSACTIONS ON IMAGE PROCESSING, vol. 13, no. 4, pp. 1–14, Apr. 2004.

[10] Z. Wang, E. P. Simoncelli, and A. C. Bovik, "Multiscale structural similarity for image quality assessment," in Conference Record of the Thirty-Seventh Asilomar Conference on Signals, Systems and Computers, 2004, 2003, vol. 2, pp. 1398–1402 Vol.2.

[11] L. Zhang, D. Zhang, X. Mou, and D. Zhang, "FSIM: A Feature Similarity Index for Image Quality Assessment," IEEE Transactions on Image Processing, vol. 20, no. 8, pp. 2378–2386, 2011.

[12] L. Zhang, D. Zhang, and X. Mou, "RFSIM: A feature based image quality assessment metric using Riesz transforms," in 2010 17th IEEE International Conference on Image Processing (ICIP), 2010, pp. 321–324.

[13] T. Acharya and A. K. Ray, "Introduction," in Image Processing, John Wiley & Sons, Inc., 2005, pp. 1–16.

[14] E. Kofidisi, N.Kolokotronis, A. Vassilarakou, S. Theodoridis and D. Cavouras, "Wavelet-based medical image compression," Future Generation Computer Systems, vol. 15, no. 2, pp. 223–243, Mar. 1999.

[15] M. Beladgham, A. Bessaid, A. Moulay-Lakhdar, M. BenAissa, A. Bassou, "MRI Image Compression using Biorthogonal CDF Wavelet Based on Lifting Scheme and SPIHT coding," Journal of Scientific Research, no. 2, pp. 225–232, 2010.

[16] "http://www.o2-wellness.com/mt-imaging.htm." .

[17] Z. Wang and Q. Li, "Information Content Weighting for Perceptual Image Quality Assessment," IEEE Transactions on Image Processing, vol. 20, no. 5, pp. 1185–1198, 2011.

[18] S. M. R. Islam, Xu Huang, and Dharmendra Sharma, "Wavelet Based Denoising Algorithm of the ECG Signal Corrupted by WGN and Poisson Noise," presented at the 12th International Symposium on Communications and Information Technologies (ISCIT 2012), Gold Coast, Australia, 2012, pp. 107–110.

Sheikh Md. Rabiul Islam received the B.Sc.in Engg. (ECE) from Khulna University, Khulna, Bangladesh in December 2003, and M.Sc. in Telecommunication Engineering from the University of Trento, Italy, in October 2009 and currently doing an PhD by Research under Faculty of Education, Science, Technology & Mathematics at University of Canberra, Australia. He joined as a Lecturer in the department of Electronics and Communication Engineering of Khulna University of Engineering & Technology, Khulna, in 2004, where he is joined an Assistant Professor in the same department in the effect of 2008. He has published 16 Journal and six International conferences. His research interests include VLSI, Wireless communications, signal & image processing, and biomedical engineering.

Xu Huang has received the B.E. and M.E. degrees and Ph.D. in Electrical Engineering and Optical Engineering prior to 1989 and the second Ph.D. in Experimental Physics in the University of New South Wales, Australia in 1992. He has earned the Graduate Certificate in Higher Education in 2004 at the University of Canberra, Australia. He has been working on the areas of the telecommunications, cognitive radio, networking engineering, wireless communications, optical communications, and digital signal processing more than 30 years. Currently he is the Head of the Engineering at the Faculty of Education, Science, Technology & Mathematics under University of Canberra, Australia. He is the Course Conveners "Doctor of Philosophy," "Masters of Information Sciences (by research)," He has been a senior member of IEEE in Electronics and in Computer Society since 1989 and a Fellow of Institution of Engineering Australian (FIEAust), Chartered Professional Engineering (CPEng), a Member of Australian Institute of Physics. He is a member of the Executive Committee of the Australian and New Zealand Association for Engineering Education, a member of Committee of the Institution of Engineering Australia at Canberra Branch. Professor Huang is Committee Panel Member for various IEEE International Conferences such as IEEE IC3PP, IEEE NSS, etc. and he has published about two hundred papers in high level of the IEEE and other Journals and international conference; he has been awarded 9 patents in Australia.

Mrs Mingyu Liao is a PhD candidate at the Faculty of Education, Science, Technology & Mathematics, University of Canberra, Australia. She is working on the infrared images in different frequency septum, namely near field, far field and middle band. She has published a few papers in above areas. She is also working related infrared images processing.

N. K. Srinath has been working many years at the Department of Computer Science and Engineering, R.V. College of Engineering, India. As an active international researcher at the computer science and engineering Dr Professor N.K. Srinath has published many high ranked research papers at the various Journals and International conferences. Professor (Dr) N. K. Srinath has been the Head of the Computer Science and Engineering for last ten years and has made significant contributions to this area.